Article

Facilitated Diffusion of Iron(II) and Dioxygen Substrates into Human H-Chain Ferritin. A Fluorescence and Absorbance Study Employing the Ferroxidase Center Substitution Y34W

Fadi Bou-Abdallah, Guanghua Zhao, Giorgio Biasiotto, Maura Poli, Paolo Arosio, and N. Dennis Chasteen

J. Am. Chem. Soc., **2008**, 130 (52), 17801-17811 • DOI: 10.1021/ja8054035 • Publication Date (Web): 04 December 2008

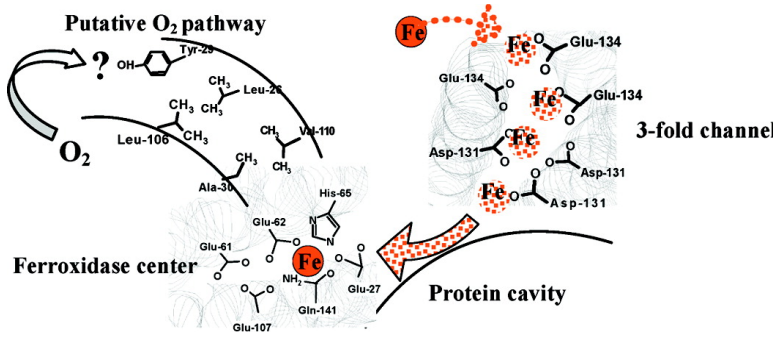

More About This Article

Additional resources and features associated with this article are available within the HTML version:

- Supporting Information
- Access to high resolution figures
- Links to articles and content related to this article
- Copyright permission to reproduce figures and/or text from this article

View the Full Text HTML

J|A|C|S
ARTICLES

Published on Web 12/04/2008

Facilitated Diffusion of Iron(II) and Dioxygen Substrates into Human H-Chain Ferritin. A Fluorescence and Absorbance Study Employing the Ferroxidase Center Substitution Y34W

Fadi Bou-Abdallah,*,† Guanghua Zhao,*,‡ Giorgio Biasiotto,§ Maura Poli,§ Paolo Arosio,§ and N. Dennis Chasteen*,‡

Department of Chemistry, State University of New York, Potsdam, New York 13676, Department of Chemistry, University of New Hampshire, Durham, New Hampshire 03824, and Chemistry Section, Faculty of Medicine, University of Brescia, 25123 Brescia, Italy

Received July 12, 2008; Revised Manuscript Received October 31, 2008; E-mail: bouabdf@potsdam.edu (F.B.-A.); gzhao318@yahoo.com.cn (G.Z.); ndc@cisunix.unh.edu (N.D.C.)

Abstract: Ferritin is a widespread iron mineralizing and detoxification protein that stores iron as a hydrous ferric oxide mineral core within a shell-like structure of 4/3/2 octahedral symmetry. Iron mineralization is initiated at dinuclear ferroxidase centers inside the protein where Fe^{2+} and O_2 meet and react to form a μ-1,2-peroxodiferric intermediate that subsequently decays to form μ-oxo dimeric and oligomeric iron(III) species and ultimately the mineral core. Several types of channels penetrate the protein shell and are possible pathways for the diffusion of iron and dioxygen to the ferroxidase centers. In the present study, UV/visible and fluorescence stopped-flow spectrophotometries were used to determine the kinetics and pathways of Fe^{2+} diffusion into the protein shell, its binding at the ferroxidase center and its subsequent oxidation by O_2. Three fluorescence variants of human H-chain ferritin were prepared in which Trp34 was introduced near the ferroxidase center. They included a control variant no. 1 (W93F/Y34W), a "1-fold" channel variant no. 2 (W93F/Y34W/Y29Q) and a 3-fold channel variant no. 3 (Y34W/W93F/D131I/E134F). Anaerobic rapid mixing of Fe^{2+} with apo-variant no. 1 quenched the fluorescence of Trp34 with a rate exhibiting saturation kinetics with respect to Fe^{2+} concentration, consistent with a process involving facilitated diffusion. A half-life of $\sim$3 ms for this process is attributed to the time for diffusion of Fe^{2+} across the protein shell to the ferroxidase center. No fluorescence quenching was observed with the 3-fold channel variant no. 3 or when Zn^{2+} was prebound in each of the eight 3-fold channels of variant no. 1, observations indicating that the hydrophilic channels are the only avenues for *rapid* Fe^{2+} access to the ferroxidase center. Substitution of Tyr29 with glutamine at the entrance of the "1-fold" hydrophobic channel had no effect on the rate of Fe^{2+} oxidation to form the μ-1,2-peroxodiferric complex ($t_{1/2} \approx 38$ ms), a finding demonstrating that Tyr29 and, by inference, the "1-fold" channels do not facilitate O_2 transport to the ferroxidase center, contrary to predictions of DFT and molecular dynamics calculations. O_2 diffusion into ferritin occurs on a time scale that is fast relative to the millisecond kinetics of the stopped-flow experiment.

Introduction

Ferritins are members of the superfamily of iron storage and detoxification proteins found throughout the animal, plant and microbial kingdoms and play key roles in the biological management of iron.[1−4] These proteins sequester excess cellular iron and, in so doing, minimize "free iron" which contributes to the generation of reactive oxygen species (ROS).[5−7] In the process of acquiring and storing iron, ferritins catalyze the simultaneous oxidation of two Fe^{2+} by a single dioxygen or hydrogen peroxide molecule by a mechanism that avoids the odd electron oxidation of iron(II) and the associated production of superoxide and hydroxyl radicals harmful to the cell.[6,7] Thus, the ferritins are not only able to efficiently harvest and store iron for later use by the cell, they also help to protect the cell against oxidative stress.[5]

All ferritins have shell-like structures (Figure 1) within which large amounts of iron ($\leq$4500 Fe) are encapsulated as a hydrous ferric oxide mineral core with a structure resembling that of ferrihydrite and displaying superparamagnetic properties.[2,3] The protein shells of mammalian ferritins are penetrated by channels and have 4/3/2 octahedral symmetry with inner and outer diameters of $\sim$80 and 120 Å, respectively, and a shell thickness of $\sim$20 Å (Figure 1). Because of its unique structural properties, the protein cavity has found application in nanotechnology as a natural template

† State University of New York, Potsdam.
‡ University of New Hampshire.
§ University of Brescia.

(1) Smith, J. L. *Crit. Rev. Microbiol.* **2004**, *30*, 173–185.
(2) Harrison, P. M.; Arosio, P. *Biochim. Biophys. Acta Bio-Energ.* **1996**, *1275*, 161–203.
(3) Chasteen, N. D.; Harrison, P. M. *J. Struct. Biol.* **1999**, *126*, 182–194.
(4) Liu, X. S.; Theil, E. C. *Acc. Chem. Res.* **2005**, *38*, 167–175.
(5) Galaris, D.; Pantopoulos, K. *Crit. Rev. Cl. Lab. Sci.* **2008**, *45*, 1–23.
(6) Zhao, G.; Bou-Abdallah, F.; Arosio, P.; Levi, S.; Janus-Chandler, C.; Chasteen, N. D. *Biochemistry* **2003**, *42*, 3142–3150.
(7) Zhao, G.; Arosio, P.; Chasteen, N. D. *Biochemistry* **2006**, *45*, 3429–3436.

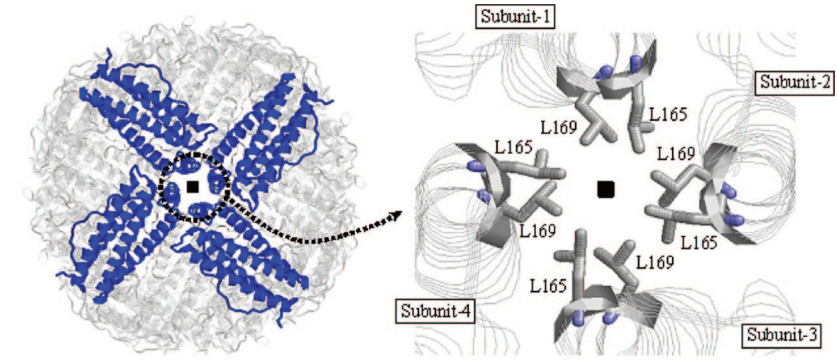

A. Four-fold Axis

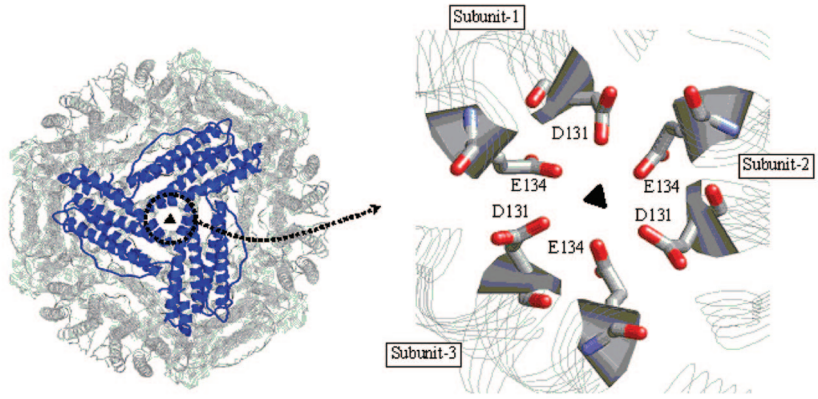

B. Three-fold Axis

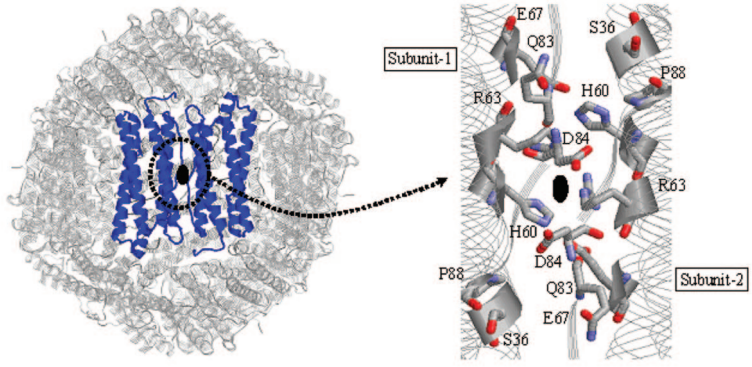

C. Two-fold Axis

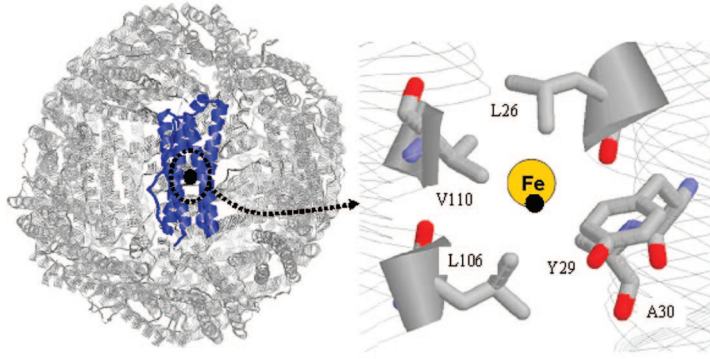

D. "One-fold" Axis

Figure 1. Ferritin protein shell with views down the (A) 4-, (B) 3-, (C) 2-, and (D) "1-fold" axes (channels) of the protein shell. The full protein shell is shown on the left with the rotation symmetry related subunits indicated in blue. An expanded view of each type of channel is shown on the right with key residues indicated. The "1-fold" rotation axis is a C_1 axis (rotation through 360°). There are an infinite number of such axes in the protein but the one shown lies along a narrow channel leading to Fe (yellow) in the A site of the ferroxidase center (see Figure 2) and thus has special significance.[9,36,37] Tyr29 extends into the exterior solution.

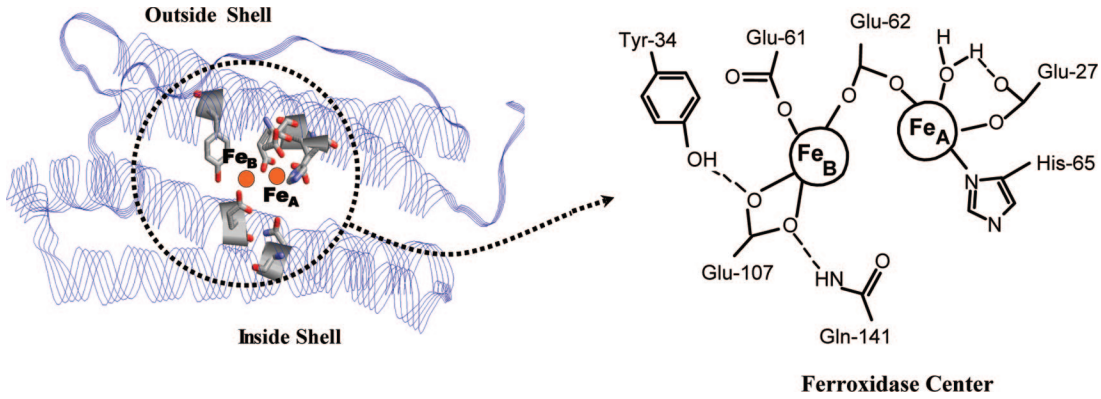

Figure 2. Ferroxidase center of human H-chain ferritin located within the four-helix bundle (left). Schematic view of the ferroxidase center (right). The ligands are those observed in the X-ray structure of Zn^{2+} bound at the ferroxidase site.[9]

for the nucleation and synthesis of a variety of metallic nanoparticles whose growth is constrained by interior size of the protein shell.[8]

Mammalian ferritins consist of 24 H- and/or L-type subunits of similar sequence and size. The pairwise oxidation of Fe^{2+} occurs at ferroxidase centers located within the four-helix bundle of the H-type subunits regardless of the source of 24mer ferritin (Figure 2).[2] The ferroxidase center is located some 7−8 Å from the inside surface of the protein shell and 12−13 Å from the exterior surface in a region of considerable hydrophobic character (Figure 2).[9] L-subunits lack ferroxidase centers and thus do not exhibit fast Fe^{2+} oxidation kinetics but facilitate nucleation of the mineral core.[2,3] The dinuclear ferroxidase centers of human H-chain homopolymer ferritin (HuHF) are composed of A and B iron binding sites of conserved amino acid ligands His65, Glu27, Glu107, Glu61 and Glu62 (Figure 2).[9,10] H-bonding residues Gln141 and Tyr34 are nearby. These ferroxidase centers differ functionally from those of the dinuclear cofactor sites of nonheme iron enzymes such as methane monooxygenase and ribonucleotide reductase. The cofactors sites of dinuclear enzymes retain and redox cycle their iron, while turning over the organic substrate to product,[11] whereas the ferroxidase center of ferritin continually turns over its iron during the catalytic cycle, releasing it to the core for storage.,[2−4]

The mechanism by which iron is sequestered within ferritin involves the diffusion of both Fe^{2+} and O_2 (or H_2O_2) into the interior of the protein, the binding and oxidation of Fe^{2+} at the ferroxidase centers to form a diferric peroxo intermediate, the release of hydrogen peroxide, and the hydrolysis and migration of the resultant Fe^{3+} to form the mineral core within the protein shell.[12−16] There are several potential pathways for Fe^{2+} entry into the protein cavity, including the eight 3-fold (Figure 1B),[17−21] the twelve 2-fold (Figure 1C),[22] and the twenty-four "1-fold" channels (Figure 1D),[9] all of which connect the interior of the protein to the outside solution. The weight of evidence, however, favors the 3-fold hydrophilic channels. For example, divalent cations have been shown by X-ray crystallography to bind within the 3-fold channel at three Asp131 and three Glu134 residues contributed by three separate subunits related by 3-fold symmetry (Figure 1B) [10,23] as well as at His118 and Cys130 residues at the outer opening of the channels.[10] Substitution of any of these residues decreases both the rate of iron uptake[17,18] and the amount of Fe^{2+} binding at the ferroxidase centers[24] and results in attenuation of core mineralization. Isothermal titration calorimetry (ITC) and kinetic measurements have shown that the mechanism of Tb^{3+} and Zn^{2+} inhibition of Fe^{2+} binding and oxidation in HuHF occurs from the binding of these metal ions in the 3-fold channels, reducing access of the Fe^{2+} to the ferroxidase centers.[20] The ligand exchange inert Cr(TREN)$(H_2O)(OH)^{2+}$ complex also blocks access of Fe^{2+} to the cavity of ferritin, presumably by binding in the channels.[21,25] In addition, localized unfolding around the 3-fold channels from the use of chaotropic agents or site-directed mutagenesis enhances the transit of iron into and out of the protein cavity.[26−28]

(8) (a) Mayes, E. L.; Mann, S. *Nanobiotechnology* **2004**, 278–287. (b) Klem, M. T.; Mosolf, J.; Young, M.; Douglas, T. *Inorg. Chem.* **2008**, *47*, 2237–2239. (c) Kasyutich, O.; Sarua, A.; Schwarzacher, W. *J. Phys. D* **2008**, *41*, 134022/1–134022/3. (d) Miura, A.; Uraoka, Y.; Fuyuki, T.; Yoshii, S.; Yamashita, I. *J. Appl. Phys.* **2008**, *103*, 074503/1−074503/10.
(9) Lawson, D. M.; Artymiuk, P. J.; Yewdall, S. J.; Smith, J. M. A.; Livingstone, J. C.; Treffry, A.; Luzzago, A.; Levi, S.; Arosio, P.; Cesareni, G.; Thomas, C. D.; Shaw, W. V.; Harrison, P. M. *Nature* **1991**, *349*, 541–544.
(10) Toussaint, L.; Bertrand, L.; Hue, L.; Crichton, R. R.; Declercq, J.-P. *J. Mol. Biol.* **2007**, *365*, 440–452.
(11) (a) Theil, E. C.; Liu, X. S.; Matzapetakis, M. *Met. Ions Life Sci.* **2008**, *4*, 327–341. (b) Schwartz, J. K.; Liu, X. S.; Tosha, T.; Theil, E. C.; Solomon, E. I. *J. Am. Chem. Soc.* **2008**, *130*, 9441–9450.
(12) Bou-Abdallah, F.; Papaefthymiou, G.; Scheswohl, D. S.; Stanga, S.; Arosio, P.; Chasteen, N. D. *Biochem. J.* **2002**, *364*, 57–63.
(13) Treffry, A.; Zhao, Z.; Quail, M. A.; Guest, J. R.; Harrison, P. M. *Biochemistry* **1995**, *34*, 15204–15213.
(14) Zhao, Z.; Treffry, A.; Quail, M. A.; Guest, J. R.; Harrison, P. M. *J. Chem. Soc., Dalton Trans.* **1997**, 3977–3978.
(15) Pereira, A. S.; Small, W.; Krebs, C.; Tavares, P.; Edmondson, D. E.; Theil, E. C.; Huynh, B. H. *Biochemistry* **1998**, *37*, 9871–9876.
(16) Waldo, G. S.; Theil, E. C. *Biochemistry* **1993**, *32*, 13262–13269.
(17) Treffry, A.; Bauminger, E. R.; Hechel, D.; Hodson, N. W.; Nowik, I.; Yewdall, S. J.; Harrison, P. M. *Biochem. J.* **1993**, *296*, 721–728.
(18) Levi, S.; Santambrogio, P.; Corsi, B.; Cozzi, A.; Arosio, P. *Biochem. J.* **1996**, *317*, 467–73.
(19) Treffry, A.; Harrison, P. M.; Luzzago, A.; Cesareni, G. *FEBS Lett.* **1998**, *247*, 268–272.
(20) Bou-Abdallah, F.; Arosio, P.; Levi, S.; Janus-Chandler, C.; Chasteen, N. D. *J. Biol. Inorg. Chem.* **2003**, *8*, 489–497.
(21) Barnés, C. M.; Theil, E. C.; Raymond, K. N. *PNAS* **2002**, *99*, 5195–5200.
(22) Michaux, M. A.; Dautant, A.; Gallois, B.; Granier, T.; d'Estaintot, B. L.; Precigoux, G. *Proteins* **1996**, *24*, 314–21.
(23) Harrison, P. M.; Ford, G. C.; Rice D. W.; Smith, J. M. A.; Treffry, A.; White, J. L. The three-dimensional structure of apoferritin. A framework controlling ferritin's iron storage and release. In *Frontiers in Bioinorganic Chemistry*; Xavier A., Ed.; VCH, Weinheim, 1986; pp 268−277.
(24) Bou-Abdallah, F.; Arosio, P.; Santambrogio, P.; Yang, X.; Janus-Chandler, C.; Chasteen, N. D. *Biochemistry* **2002**, *41*, 11184–11191.
(25) Barnés, C. M.; Petoud, S.; Cohen, S. M.; Raymond, K. N. *J. Biol. Inorg. Chem.* **2003**, *8*, 195–205.

The stoichiometry and association constant of Fe^{2+} binding to the ferroxidase centers of HuHF have been determined by ITC under equilibrium conditions,[24] but limited information is available on the dynamics of Fe^{2+} transfer across the protein shell to these centers. The overall process must occur in less than ~50 ms based on sequential stopped-flow spectroscopy[29] employing 1,10-phenanthroline to measure unbound Fe^{2+} and on the time required for the peroxodiferric intermediate to form.[29−33] An attempt has been made to measure the time for Fe^{2+} diffusion into horse spleen ferritin by following the generation of Prussian Blue inside the protein cavity but a much slower rate was obtained than the aforementioned studies suggest.[34]

To date, the pathways and rates of O_2 entry into ferritin have been little explored. Based on the early crystallography of the horse spleen protein, the six 4-fold hydrophobic channels lined with leucine residues were suggested as possible avenues for diffusion of dioxygen into the protein interior (Figure 1A).[35] However, the more recent X-ray structure of *E. coli* bacterial ferritin (EcFtnA) has identified 24 short hydrophobic channels along the "1-fold axis" of each subunit that penetrate directly through the subunit to the ferroxidase center and are potential pathways for O_2 entry (Figure 1D).[36] Similar hydrophobic channels are found in the H-chain subunit of human ferritin and are composed of residues Leu26, Ala30, Leu106, and Val110.[37] Tyr29, a conserved residue, is located at the entrance to the "1-fold" channel and extends into the external solution (Figure 1D). Density functional theory (DFT) and molecular dynamics calculations have led to the hypothesis that Tyr29 interacts with O_2 in the bulk solution thereby directing it into the "1-fold" channel where it diffuses to the ferroxidase center.[37]

Kinetic studies of the interaction of Fe^{2+} with HuHF are difficult to carry out because of the insensitivity of the UV−visible and fluorescence spectra of the WT protein to Fe^{2+} binding.[14,38] The single tryptophan residue (Trp93) per H-subunit in HuHF is situated ~17 Å from the ferroxidase center, and this large distance probably accounts for the lack of an effect of Fe^{2+} binding on the intrinsic fluorescence and absorption properties of the protein.

The present study was undertaken to measure directly the rates of Fe^{2+} and O_2 diffusion to the ferroxidase center of HuHF. Toward this end, three variants were prepared in which a fluorescent reporter group was introduced near the ferroxidase center through the substitution Y34W. The only tryptophan in the wild-type protein (Trp93) was simultaneously eliminated by the substitution W93F to avoid contributions from this residue to the observed fluorescence. Variant no. 1 (W93F/Y34W) served as a "WT" control. Variant no. 2 (W93F/Y34W/Y29Q) was used to test the importance of Tyr29 for O_2 diffusion into the protein and variant no. 3 (W93F/Y34W/D131I/E134F) to test the importance of the 3-fold channels for *rapid* Fe^{2+} diffusion into the protein. Stopped-flow fluorescence and stopped-flow absorbance spectrophotometries were employed to measure the kinetics of Fe^{2+} and O_2 arrival at the ferroxidase center and the subsequent oxidation of the iron.

Our experiments show that Fe^{2+} rapidly traverses the protein shell ($t_{1/2} \approx 3$ ms) via the 3-fold channels and not by another rapid pathway. Diffusion into ferritin shows saturation kinetics characteristic of facilitated diffusion and is consistent with a model in which Fe^{2+} binds initially in the 3-fold channels and then migrates to the protein interior and ultimately to the ferroxidase center. When Fe^{2+} is prebound anaerobically to the ferroxidase center, the rate of Fe^{2+} oxidation upon rapid mixing of the Fe^{2+}−protein complex with an aerobic solution is unaffected by the substitution Y29Q, a result indicating that Tyr29 is unimportant mechanistically for oxygen transport. The data further indicate that O_2 must reach the ferroxidase center with or without Tyr29 present in a time much shorter than the observed half-life of 38 ms for Fe^{2+} oxidation when Fe^{2+} is prebound to the ferroxidase centers prior to the introduction of O_2.

Materials and Methods

Reagent grade ferrous sulfate was obtained from Baker Scientific Inc. (Phillipsburg, NJ) and Mops hemisodium buffer from Research Organics (Cleveland, OH). The constructs for variant no. 1 (W93F/Y34W), variant no. 2 (W93F/Y34W/Y29Q), and variant no. 3 (W93F/Y34W/D131I/E134F) were prepared by oligonucleotide site-directed mutagenesis on the plasmid pET-HuHF encoding human H-ferritin[39] by using QuikChange kit (Stratagene). The plasmids were verified by direct DNA sequencing. The proteins were expressed in transformed *E. coli* and purified as previously described.[39] The concentrations of all three variants on a 24mer basis were determined by Advanced Protein Assay (http://cytoskeleton.com) using BSA as a standard. Molar absorptivities at 280 nm for variants no. 1 and 2 were estimated to be 17 000 and 14 000 M^{-1} cm^{-1} per subunit, respectively, which compare with predicted values of 17 400 and 15 900 M^{-1} cm^{-1} based on their amino acid sequences (using the ProtParam tool at http://ca.expasy.org) and with the value of 23 000 M^{-1} cm^{-1} per subunit for the WT protein.[40] Circular dichroism (CD) spectra and melting curves for variant no. 1 and the WT protein were very similar (Figures S1 and S2), indicating that the mutation caused no major structural change in the protein. All of the variants eluted as 24mers on size exclusion chromatography. The protein was rendered iron free by continuous flow anaerobic dialysis in the presence of sodium dithionite and 2,2′-bipyridyl.[41,42]

CD spectra were measured on a Jasco J815 instrument. Isothermal titration calorimetry measurements were made with a CSC Model 4200 calorimeter as previously described.[24] Equilibrium fluorescence measurements were performed on a Varian Cary

(26) Liu, X.; Jin, W.; Theil, E. C. *PNAS* **2003**, *100*, 3653–3658.
(27) Liu, X.; Theil, E. C. *Acc. Chem. Res.* **2005**, *38*, 167–175.
(28) Theil, E. C.; Takagi, H.; Small, G. W.; He, L.; Tipton, A. R.; Danger, D. *Inorg. Chim. Acta* **2000**, *297*, 242–251.
(29) Treffry, A.; Zhao, Z.; Quail, M. A.; Guest, J. R.; Harrison, P. M. *Biochemistry* **1997**, *36*, 432–441.
(30) Moënne-Loccoz, P.; Krebs, C.; Herlihy, K.; Edmondson, D. E.; Theil, E. C.; Huynh, B. H.; Loehr, T. M. *Biochemistry* **1999**, *38*, 5290–5295.
(31) Bou-Abdallah, F.; Zhao, G.; Mayne, H. R.; Arosio, P.; Chasteen, N. D. *J. Am. Chem. Soc.* **2005**, *127*, 3885–3893.
(32) Liu, X.; Theil, E. C. *PNAS* **2004**, *101*, 8557–8562.
(33) Zhao, G.; Su, M.; Chasteen, N. D. *J. Mol. Biol.* **2005**, *352*, 467–477.
(34) Zhang, B.; Watt, R. K.; Gálvez, N.; Dominguez-Vera, J.; Watt, G. D. *Biophys. Chem.* **2006**, *120*, 96–105.
(35) Ford, G. C.; Harrison, P. M.; Rice, D. W.; Smith, J. M. A.; Treffry, A.; White, J. L.; Yariv, J. *Philos. Trans. R. Soc. London* **1984**, *304*, 551–565.
(36) Stillman, T. J.; Hempstead, P. D.; Artymiuk, P. J.; Andrews, S. C.; Hudson, A. J.; Treffry, A.; Guest, J. R.; Harrison, P. M. *J. Mol. Biol.* **2001**, *307*, 587–603.
(37) Ciacchi, L. C.; Payne, M. C. *Chem. Phys. Lett.* **2004**, *390*, 491–495.
(38) Yang, X.; Chen-Barrett, Y.; Arosio, P.; Chasteen, N. D. *Biochemistry* **1998**, *37*, 9743–9750.
(39) Santambrogio, P.; Cozzi, A.; Levi, S.; Rovida, E.; Magni, F.; Albertini, A.; Arosio, P. *Protein Expr. Purif.* **2000**, *19*, 212–218.
(40) Zhao, G.; Bou-Abdallah, F.; Yang, X.; Arosio, P.; Chasteen, N. D. *Biochemistry* **2001**, *40*, 10832–10838.
(41) Bauminger, E. R.; Harrison, P. M.; Hechel, D.; Nowik, I.; Treffry, A. *Biochim. Biophys. Acta* **1991**, *1118*, 48–58.
(42) Treffry, A.; Hirzmann, J.; Yewdall, S. J.; Harrison, P. M. *FEBS Lett.* **1992**, *302*, 108–112.

Eclipse fluorimeter or on a SLM Aminco-Bowman Series 2 luminescence spectrometer (AB2). Titrations of 1.0 μM variant no. 1 in 100 mM Mops pH 7.15 at 25 °C with 0−48 μM $FeSO_4$ were carried out under an argon atmosphere in a 1-cm gas-tight fluorescent cell fitted with a septum. To test the ability of O_2 to quench the fluorescence of Trp-34 of variant no. 1, a 100% O_2 atmosphere was introduced over the stirred anaerobic apoprotein solution with the fluorescence monitored before and after introduction of O_2.

The kinetics of fluorescence quenching was performed with the pneumatic drive Hi-Tech SFA-20 M stopped-flow accessory interfaced to the Cary Eclipse fluorimeter or to the SLM Aminco-Bowman Series 2 luminescence spectrometer which acquire a data point every 12.5 or 0.300 ms, respectively. The AB2 spectrometer was used for the fastest reactions encountered in this work. The dead times of the two instruments were determined to be 9.2 ± 0.2 and 3.7 ± 0.1 ms, respectively, using the *N*-acetyltryptophanamide (NATA) and *N*-bromo-succinamide (NBS) test reaction.[43] The dead times take into account both the mixing time and software delay for the two instruments. The rate constant of the test reaction run on the SFA-20M/Eclipse apparatus at NATA and NBS concentrations of 5.00 and 50.0 μM, respectively, was determined to be 34.8 ± 0.7 s^{-1} ($t_{1/2}$ = 19.9 ± 0.4 ms) from data measured over four half-lives (Figure S3) which compares favorably with the literature value of 37.4 s^{-1} ($t_{1/2}$ = 18.5 ms) under identical conditions.[43] The test reaction run on the SFA-20M/Aminco-Bowman apparatus at NATA and NBS concentrations of 5.00 and 200 μM, respectively, gave a rate constant of 152 ± 2 s^{-1} ($t_{1/2}$ = 4.55 ms) (Figure S4) which is close to the literature value of 155 s^{-1} ($t_{1/2}$ = 4.47 ms) under the same conditions.[43]

The kinetics of Fe^{2+} binding to apo-variants no. 1, 2, and 3 were performed anaerobically. The stopped-flow apparatus was fitted with a polyvinylchloride bag specifically designed by the manufacturer for anaerobic work and flushed with high-purity argon overnight before use. All buffers and Fe^{2+} solutions were made oxygen-free by extensive bubbling with moist argon overnight prior to use. Moist argon was passed over the stirred apoprotein solution overnight to remove oxygen. Then equal volumes (140 μL) of a 12−72 μM $FeSO_4$ solution, pH ≈ 2, acidified with 3 N HCl with or without 25 mM NaCl (as indicated by the presence or absence of NaCl in the figure legends) and apoprotein (1.0 − 3,0 μM) in Mops buffer (50−100 mM), pH 7.15, were rapidly mixed in the thermostatted sample compartment and pushed through the 80 μL quartz stopped-flow cuvette. Path lengths for excitation and emission were 1.0 and 0.2 cm at wavelengths of 280 and 324 nm, respectively. A slit width of 5 nm for excitation and 10 nm for emission was used with the Cary Eclipse and 5 nm for both excitation and emission slits for the AB2.

To ensure that the Fe^{2+} solutions remained reduced before mixing with the apoprotein, they were prepared anaerobically in pH ≈ 2 water (acidified with 3 N HCl) in the absence of buffer as done in all previous stopped-flow kinetics studies of ferritins.[16,29,31,34] The low pH helps to stabilize the Fe^{2+} from slow oxidation due to traces of O_2 in the solution (<0.5 μM as measured by Clark electrode oximetry) during the time required to prepare the stopped-flow system for each kinetic run. However, this protocol causes a 2-fold drop in Mops buffer hemisodium concentration at the start of the reaction from 50 mM to 25 mM upon rapid mixing of the protein and iron solutions and a corresponding decrease in ionic strength from μ = 25 to 12.5 mM. Therefore, the influence of ionic strength on the fluorescence and absorption spectra of the apoprotein and its iron complex was investigated. No effect was found. The change in ionic strength on the kinetics of Fe^{2+} diffusion was also investigated. In these experiments, the Fe^{2+} solution at pH ≈ 2 was prepared with or without added 25 mM NaCl (μ = 25 mM) while the apoprotein solution contained only 50 mM Mops (μ = 25 mM), pH 7.15. The first-order rate constants for fluorescence decay were only ∼10% larger when NaCl was present in the Fe^{2+} solution than when it was absent, indicating that the 2-fold drop in ionic strength upon mixing has a minimal effect on the observed kinetics.

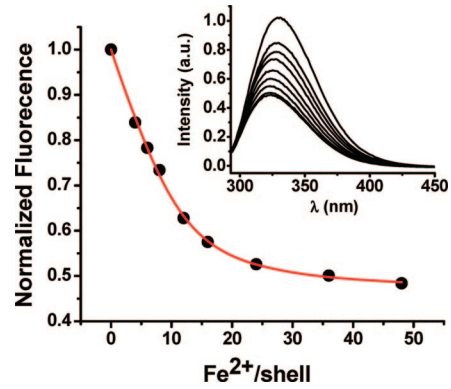

Figure 3. Fluorescence quenching upon Fe^{2+} binding anaerobically to variant no. 1. Inset: Family of spectra. The red line is the fit of eq 1 to these data with n_F = 11.7 ± 0.7, K_F = (1.1 ± 0.2) × 10^6 and I_∞ = 0.460 ± 0.009 (95% confidence level). The average and standard deviations obtained for four titrations are n_F = 11.4 ± 2.1 and K_F = (1.3 ± 0.8) × 10^6 M^{-1}. Conditions: $\lambda_{Ex.}$ = 280 nm, $\lambda_{Em.}$ = 324 nm, slits for excitation and emission of 4 and 8 nm, respectively, 1.0 μM apoprotein, 0 − 48 μM $FeSO_4$, 50 mM Mops, pH 7.15, 25 °C.

In the experiments to measure oxidation of prebound Fe^{2+} by O_2, a 140 μL volume of deionized water saturated with 100% O_2 was rapidly mixed with the same volume of anaerobic 3.0 μM variants no. 1 and 2 containing 48 Fe^{2+}/shell in 100 mM Mops buffer pH 7.15. As indicated in the figure captions, multiple traces were averaged to improve the signal-to-noise ratio of the data prior to analysis.

Stopped-flow, multiple-wavelength absorption studies were carried out with the Hi-Tech SFA-20 M apparatus interfaced to a J&M Tidas diode array spectrometer with data acquisition every 2.5 ms in the wavelength range 290−800 nm. The peroxodiferric species formed during oxidation of Fe^{2+} was monitored by its absorbance value at 650 nm. The spectrophotometer baseline was determined prior to each kinetic run with a cuvette containing equal volumes of apoprotein in buffer and acidic H_2O (pH ≈ 2).

Analysis of the kinetics was carried out as recently described.[31,33] The data were fitted to derived kinetic equations programmed into Origin, version 7.0, software (OriginLab, Inc.). Stated errors are at the 95% confidence level from the goodness-of-fit unless stated otherwise. The dead time was added to all measured times post triggering of data collection and a zero point at zero-time was added to all data sets.

Results

Fluorescence Quenching of Variant No. 1 by Fe^{2+} Binding. The fluorescence spectra of variant no. 1 (W93F/Y34W) containing different amounts of Fe^{2+} are shown in Figure 3 (inset). The intensites of fluorescence and absorption spectra were found to be independent of the ionic strengths of 12.5−25 mM employed in this work (Materials and Methods). Maximal emission occurs at 324 nm for the apoprotein, indicating that most of the observed fluorescence is contributed by the sole tryptophan residue Trp34. Anaerobic addition of Fe^{2+} causes a blue shift in the band maximum to 317 nm, a result suggestive of movement of the Trp34 to a more hydrophobic environment upon binding of iron to the protein.[44] To establish the binding stoichiometry, the apoprotein was titrated anaerobically with

(43) Peterman, B. F. *Anal. Biochem.* **1979**, *93*, 442–444.

(44) Lakowicz, J. R. *Principles of Fluorescence Spectroscopy*; Klewer Academic: New York, 1999; pp 454−456.

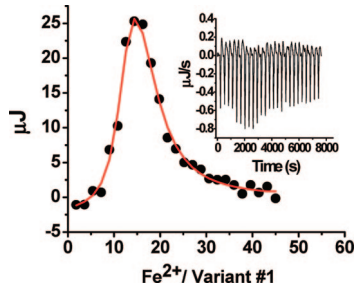

Figure 4. Calorimetric titration of variant no. 1 (W93F/Y34W) with Fe^{2+} under anaerobic conditions. Plot of integrated heat versus Fe^{2+}/variant no. 1 ratio. Inset: Raw data. The red line is the result of curve fitting to two independent classes of binding sites with $n_1 = 12.0 \pm 0.7$, $K_1 = (3.9 \pm 2.2) \times 10^6$ M^{-1} and $\Delta H_1^o = -0.45 \pm 0.17$ kJ mol^{-1}, corresponding to $\Delta G_1^o = -37.6 \pm 1.5$ kJ mol^{-1} and $\Delta S_1^o = 125 \pm 5$ J K^{-1} mol^{-1}, and $n_2 = 6.8 \pm 1.90$, $K_2 = (1.5 \pm 0.5) \times 10^5$ M^{-1} and $\Delta H_2^o = 14.0 \pm 7.3$ kJ mol^{-1}, corresponding to $\Delta G_2^o = -29.5 \pm 0.8$ kJ/mol and $\Delta S_2^o = 146 \pm 25$ J K^{-1} mol^{-1}. Conditions: 3 μM protein in 0.1 M Mops and 2 mM $Na_2S_2O_4$, pH 7.05. The Fe^{2+} solution was prepared in anaerobic 0.1 M Mops, 2 mM $Na_2S_2O_4$, pH 7.05. $Na_2S_2O_4$ helps to maintain an oxygen-free solution during the titration. Its presence does not affect Fe^{2+} binding to the protein.[24]

Fe^{2+} while monitoring the fluorescence. The addition of increments of Fe^{2+} to variant no. 1 up to ~12 Fe^{2+}/shell resulted in marked quenching of the protein fluorescence, beyond which quenching was less pronounced (Figure 3). The data were fitted to eq 1 (Supporting Information) for the binding of Fe^{2+} to n_F independent ferroxidase sites on the protein.

$$I = I_o - \frac{(I_o - I_\infty)}{2n_F[P]_o} \cdot [1/K_F + [Fe]_o + n_F[P]_o - \sqrt{(1/K_F + [Fe]_o + n_F[P]_o)^2 - 4n_F[Fe]_o[P]_o}] \quad (1)$$

Here K_F is the site association constant, $[P]_o$ and $[Fe]_o$ are the 24-mer protein and iron concentrations, and I_o and I_∞ are the relative fluorescence intensities in the absence of Fe^{2+} and in the presence of Fe^{2+} when the sites are fully saturated, respectively. Average and standard deviation for four titrations were $n_F = 11.4 \pm 2.1$ and $K_F = (1.3 \pm 0.8) \times 10^6$ M^{-1} (range $= (0.7-2.6) \times 10^6$ M^{-1}). The observed stoichiometry of $n_F \approx 12$ from the fluorescence titrations was confirmed by an anaerobic UV spectrometric titration of the apoprotein with Fe^{2+} (Figure S5). Isothermal titration calorimetry, which accounts for all binding that produces a measurable heat, was also carried out (Figure 4). Two classes of binding sites were observed ($n_1 = 12.0 \pm 0.7$ and $K_1 = (3.9 \pm 2.2) \times 10^6$ M^{-1}; $n_2 = 6.8 \pm 1.9$ and $K_2 = (1.5 \pm 0.5) \times 10^5$). The stoichiometry and equilibrium constant of the strong class of binding sites are the same within experimental uncertainty as those obtained from the fluorescence quenching titration (Figure 3). The weaker binding sites ($n_2 = 6.8 \pm 1.9$) observed by ITC are attributed to the eight hydrophilic channels (vide infra).[20,24] Thus, variant no. 1 binds about half as much Fe^{2+} at the ferroxidase centers as does the WT protein, which binds 24 Fe^{2+}, one at each ferroxidase center under similar conditions.[24] Fe^{2+} binding most likely occurs at the His65-containing A-site of the ferroxidase center of Figure 2 as previous studies suggest.[10,24,29] (In constrast, both the A and B sites of the frog M protein are occupied by Fe^{2+}.[11b])

Pathway of Fe^{2+} Entry into Ferritin. To probe the pathway for iron entry into ferritin, stopped-flow fluorescence quenching experiments were performed on the 3-fold channel variant no. 3 (Y34W/W93F/D131I/E134F) (Figure 5). The intrinsic fluorescence of channel variant no. 3 was not quenched when the

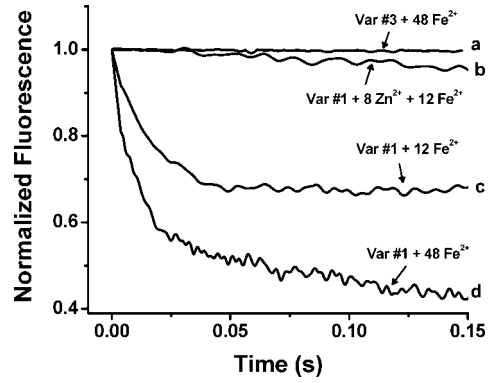

Figure 5. Stopped-flow fluorescence quenching by the anaerobic addition of 48 Fe^{2+} to apo-variant no. 3 (curve a), of 12 Fe^{2+} to apo-variant no. 1 with 8 Zn^{2+} bound (curve b), of 12 Fe^{2+} to apo-variant no. 1 (curve c), and of 48 Fe^{2+} to apo-variant no. 1 (curve d). Each curve is the average of 6 to 9 runs. Final conditions: 0.5 μM protein in 25 mM Mops hemisodium salt, 12.5 mM NaCl, pH 7.15, 25 °C. The Fe^{2+} solution was prepared in anaerobic 25 mM NaCl, pH ≈ 2.5.

protein was rapidly mixed with an Fe^{2+} solution (48 Fe/shell) either anaerobically (curve a) or aerobically (not shown) as also found in a control experiment where variant no. 1 was rapidly mixed with just H_2O (not shown). In contrast, the intrinsic fluorescence was greatly quenched when variant no. 1 was rapidly mixed anaerobically with 48 Fe^{2+} (curve d), suggesting that in the channel variant no. 3, Fe^{2+} is unable to reach the ferroxidase center within the time frame of the stopped-flow experiment. Because the four amino acid substitutions in variant no. 3 conceivably could render the ferroxidase center incapable of binding Fe^{2+}, measurements were also undertaken with variant no. 1 having eight Zn^{2+} bound per protein, one in each of the eight 3-fold channels.[20] A marked reduction in quenching was observed upon the addition of Fe^{2+} compared to the control in the absence of Zn^{2+} (Figure 5, cf. curves b and c), a result confirming that the 3-fold channels are the primary pathways for rapid Fe^{2+} entry into the protein shell.

The slow further quenching beyond ~20 ms observed with variant no. 1 containing 48 Fe^{2+}/shell (Figure 5, curve d) is attributed to trace O_2 in the solution slowly oxidizing some of the Fe^{2+} to Fe^{3+} (Fe^{3+} binding quenches the fluorescence about twice as much as Fe^{2+} binding). This additional slow quenching was not observed in the spectrometric titrations (c.f. Figure 3) where anaerobic conditions could be maintained better than in the stopped-flow experiments.

Kinetics of Fe^{2+} Diffusion to the Ferroxidase Site. The rate of Fe^{2+} binding to the ferroxidase center was determined by fluorescence quenching stopped-flow measurements in which Fe^{2+} was rapidly mixed anaerobically with apo-variant no. 1 at Fe^{2+}/shell ratios ranging from 4:1 to 48:1. The time courses for fluorescence quenching show simple first-order decay (Figure 6) with little influence of ionic strength on the rates (Materials and Methods). The samples containing 36 and 48 Fe^{2+}/shell show a second phase that is 30 − 40 times slower than the first phase due to gradual oxidation of the iron. A slow second phase was also seen for the other samples when examined on a much longer time scale (not shown). We focus on the rapid-first phase due to Fe^{2+} binding at the ferroxidase centers.

The initial rate of quenching shows saturation kinetics with respect to total Fe^{2+} concentration (Figure 7), a phenomenon characteristic of facilitated diffusion in membranes whereby

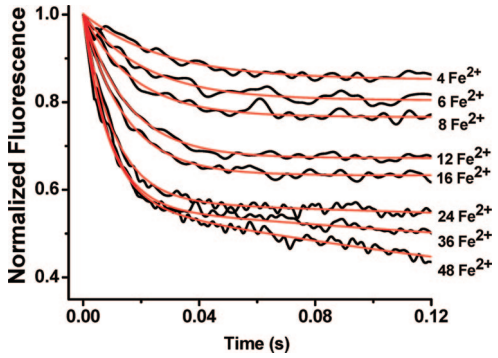

Figure 6. Stopped-flow fluorescence quenching by Fe^{2+} binding to variant no. 1. The corresponding fits to the data are shown in red. Each curve is the average of 6−9 kinetic runs. The data shown are truncated at 0.12 s but were gathered and fitted to 2.0 s. The fits are single exponentials, $I = (I_o - I_\infty)e^{k_{obs}t} + I_\infty$, except for the 36 and 48 Fe^{2+}/shell samples where a second more slowly decaying exponential was used. Fitting to the initial rapid decay gives $k_{obs} = 46.6 \pm 1.0$, 52.0 ± 1.5, 56.9 ± 1.1, 64.9 ± 0.6, 69.9 ± 1.0, 81.0 ± 2.1, 89.8 ± 2.3, and 94.4 ± 2.5 s^{-1} for the 4 Fe^{2+} through 48 Fe^{2+}/shell samples, respectively, with errors at the 95% confidence level. Final conditions: protein concentration 0.5 μM in 25 mM Mops, 12.5 mM NaCl, pH 7.15 at 25 °C with Fe^{2+} added in various amounts as indicated.

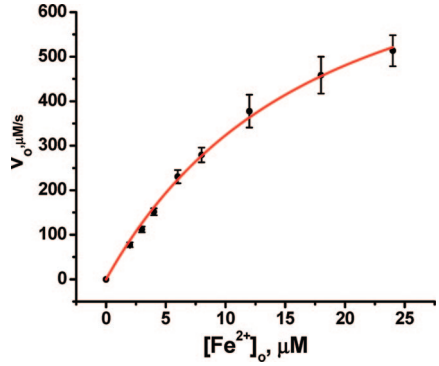

Figure 7. Plot of the initial velocity v_0 for Fe^{2+} arrival at the ferroxidase center versus total Fe^{2+} concentration. The initial velocity v_0 is given by v_o (μM/s) = $\alpha k_{obs}(I_o - I_\infty)$ where the values of $k_{obs}(s^{-1})$ and $I_o - I_\infty$ are from curve fitting of each kinetic trace in Figure 6. Error bars are from the propagated errors in k_{obs} and $I_o - I_\infty$. α is the proportionality constant between the maximal concentration of Fe^{2+} bound at the ferroxidase centers and the maximal degree of fluorescence quenching, $I_o - I_\infty$, namely $\alpha = 6$ μM $Fe^{2+}/0.54 = 11.1$ μM (Supporting Information). Fitting of the unweighted data (red line) according to eq 3 with the concentration of channels $[C]_o = 4$ μM gives $K_C = (7.0 \pm 0.7) \times 10^4$ M^{-1} and $k_d = 216 \pm 12$ s^{-1} (95% confidence level).[48]

complexation and transport of the diffusant occurs.[45,46] Formally, facilitated diffusion can be modeled by a scheme analogous to that for Michaelis−Menten enzyme kinetics (eq 2).[45,46] Here the free Fe^{2+} in the bulk solution is

$$Fe + C \overset{K_C}{\rightleftharpoons} Fe_C \overset{k_d}{\rightarrow} Fe_F \qquad (2)$$

designated as Fe, the 3-fold hydrophilic channels as C, iron bound in the channels as Fe_C and iron bound at the ferroxidase site as Fe_F. K_C represents the equilibrium constant for Fe^{2+} binding in the channels. k_d is the apparent rate constant for diffusion from the channel binding site to the ferroxidase center.

We assume that the first step is a rapid pre-equilibrium. Because in our experiments, the concentrations of the Fe^{2+} and channels are comparable, the usual assumption in Michaelis−Menten kinetics that substrate is in excess does not apply and the initial rate as a function of added Fe^{2+} ($[Fe]_o$) takes on the following form (Supporting Information).[47]

$$v_o = k_d[FeC] = k_d\frac{1/K_C + [Fe]_o + [C]_o - \sqrt{(1/K_C + [Fe]_o + [C]_o)^2 - 4[C]_o[Fe]_o}}{2} \qquad (3)$$

In eq 3 the concentration of 3-fold channels sites $[C]_o$ is eight times the protein concentration. Curve fitting of the data in Figure 7 according to eq 3 gives $K_C = (0.70 \pm 0.07) \times 10^5$ M^{-1} and $k_d = 216 \pm 12$ s^{-1}, corresponding to a minimum half-life of 3.2 ms (at saturating Fe^{2+} concentration) for Fe^{2+} to arrive and bind at the ferroxidase center (more later).[48] The value of K_C from the kinetic analysis is similar to that obtained by ITC for Fe^{2+} binding in the channels, i.e., $(0.7 \pm 0.07) \times 10^5$ versus $(1.5 \pm 0.5) \times 10^5$ M^{-1}.

Fluorescence Quenching Kinetics of Variants No. 1 and 2 from O_2 Oxidation of Prebound Fe^{2+}. To determine whether Tyr29 plays an important role in O_2 transport to the ferroxidase center, stopped-flow experiments were carried out in which anaerobic solutions of variants no. 1 and 2 prebound with Fe^{2+} (48 Fe^{2+} added per shell) were rapidly mixed with 100% O_2 saturated water. Fe^{2+} oxidation by O_2 resulted in rapid quenching of fluorescence in a similar fashion for both proteins (Figure 8). Whereas a single Fe^{2+} binds to the ferroxidase center at the A-site, both sites are occupied by Fe^{3+} following oxidation.[14,15,24,29−31] After attempts to fit the data to several different models, the observed fluorescence quenching curves were best described by the standard two-step consecutive first-order reaction pathway as per eq 4

$$A \overset{k_1}{\rightarrow} B \overset{k_2}{\rightarrow} C \qquad (4)$$

In this model, species A corresponds to a colorless "$Fe^{2+}-O_2-$protein" complex rapidly formed at the ferroxidase center that converts to the peroxodiferric dimer B through a first-order process with a rate constant k_1 as previously discussed.[31] The unstable intermediate B then decays to a μ-oxodiferric dimer, species C, with a rate constant k_2. The total fluorescence intensity, $I(\lambda, t)$, of the reaction mixture as a function of time was fitted to the following equation for multiple species:

$$I(\lambda,t) = I_A(\lambda)[A(t)] + I_B(\lambda)[B(t)] + I_C(\lambda)[C(t)] + I(\lambda,\infty) \qquad (5)$$

where the I_i terms are molar intensity constants for the intrinsic fluorescence of species A, B, and C at the specified wavelength. The standard equations for the concentrations $[A(t)]$, $[B(t)]$, and $[C(t)]$ as a function of time for the consecutive reaction $A \rightarrow B \rightarrow C$ are given elsewhere[31] and found in most standard physical chemistry texts. The data in Figure 8 conform well to eq 5, giving fitted values of the apparent first-order rate constants for variant no. 1 of $k_1 = 19.0 \pm 3.1$ and $k_2 = 1.86 \pm 0.04$ s^{-1}

(45) Weiss, T. F. *Cellular Biophysics, Vol. 1: Transport*; MIT Press: Cambridge, MA, 1996; Chapters 3 and 6.
(46) Keener, J.; Sneyd, J. *Mathematical Physiology*; Springer: New York., 1998; pp 38−48.
(47) Segel, I. H. *Enzyme Kinetics*; Wiley-Interscience: New York, 1975; pp 72−74.
(48) Fitting of the data to eq 3 with each data point weighted by its error bar σ_i ($w_i = 1/\sigma_i^2$) gave $K_C = (5.2 \pm 1.1) \times 10^4$ M^{-1} and $k_d = 252 \pm 36$ (95% confidence level) which are within the error of the values from the unweighted fitting.

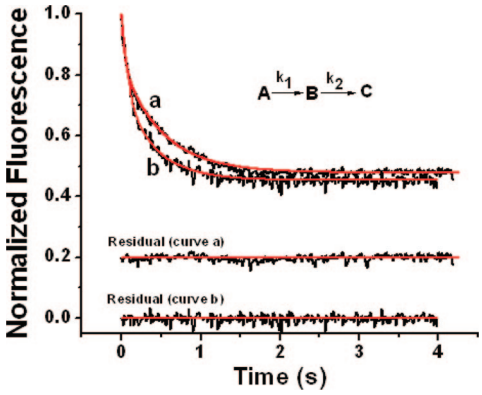

Figure 8. Stopped-flow fluorescence quenching by O_2 oxidation of Fe^{2+} prebound to variants no. 1 (curve a) and 2 (curve b) containing 48 Fe^{2+}/shell. Fitted curves are shown in red. The rate constants and intrinsic fluorescence constants for variant no. 1 from curve-fitting (curve a) are $k_1 = 19.0 \pm 3.1\ s^{-1}$ and $k_2 = 1.86 \pm 0.04\ s^{-1}$, $I_A = 1.01 \pm 0.02\ \mu M^{-1}$ on a per iron dimer basis, $I_B = 0.655 \pm 0.021\ \mu M^{-1}$ dimer, and $I_C = 0.0425 + 0.0012\ \mu M^{-1}$ dimer (curve a); and for variant no. 2 (curve b) are $k_1 = 16.6 \pm 2.3\ s^{-1}$ and $k_2 = 2.38 \pm 0.15\ s^{-1}$, $I_A = 0.711 \pm 0.011\ \mu M^{-1}$ dimer, $I_B = 0.320 \pm 0.030\ \mu M^{-1}$ dimer, and $I_C = 0.0158 \pm 0.0013\ \mu M^{-1}$ dimer (curve b) from eq 5 with the equations for the concentrations of species given elsewhere.[31] The residual is the difference between the fitted and experimental curves. The stated rate constants and associated errors are averages and standard deviations, respectively, from curve fits to three separate kinetic runs. The observed quenching kinetics is from the oxidation of the prebound Fe^{2+} and not from the binding of Fe^{2+} itself. Final conditions: anaerobic 1.5 μM apo-variants containing 48 Fe^{2+}/shell in 50 mM Mops pH 7.15 rapidly mixed with H_2O saturated with 100% O_2, 25 °C.

(curve a) and for variant no. 2 of $k_1 = 16.6 \pm 2.3$ and $k_2 = 2.38 \pm 0.15\ s^{-1}$ (curve b). The values of k_1 for formation of the peroxodiferric intermediate for both variants no. 1 and 2 are identical within the experimental uncertainty, indicating that the substitution Y29Q has no significant effect on the kinetics of iron oxidation. Thus, O_2 arrival at the ferroxidase center is not limiting the rate of Fe^{2+} oxidation in these proteins. We conclude that Tyr29 does not play a significant role in facilitating O_2 diffusion to the ferroxidase center, contrary to theoretical prediction.[37]

UV−Vis Absorption Kinetics of Variants No. 1 and 2 from O_2 Oxidation of Prebound Fe^{2+}. UV−visible stopped-flow spectrophotometry was carried out under the same conditions as the fluorescence experiments discussed above (Figure 9). Again the model $A \rightarrow B \rightarrow C$ gives the best description of the kinetics. The blue peroxodiferric intermediate B has an absorbance maximum at ~650 nm where the kinetics were monitored (Figure 9). The data were curve-fitted according to eq 6 for the absorbance $Y(\lambda,t)$ as a function of time where the ε_i correspond to molar absorptivities of species B and C at 650 nm as described elsewhere.[31,33]

$$Y(\lambda,t) = \varepsilon_B(\lambda)[B(t)] + \varepsilon_C(\lambda)[C(t)] \quad (6)$$

Curve fitting yielded $k_1 = 18.4 \pm 0.4$ and $k_2 = 1.29 \pm 0.02\ s^{-1}$ for variant no. 1 (Figure 9A) and $k_1 = 17.5 \pm 0.6$ and $k_2 = 2.49 \pm 0.06\ s^{-1}$ for variant no. 2 (Figure 9B), respectively (95% confidence level). The rate constants obtained from fitting the absorbance and fluorescence stopped-flow data are generally very similar (Figures 8 and 9). However, we consider the rate constants from the absorbance data of Figure 9 to be more accurate because the formation and decay of the peroxo intermediate B are measured directly without significant contributions to the 650 nm absorbance from the other species. Again the rate constant k_1 for formation of the peroxo

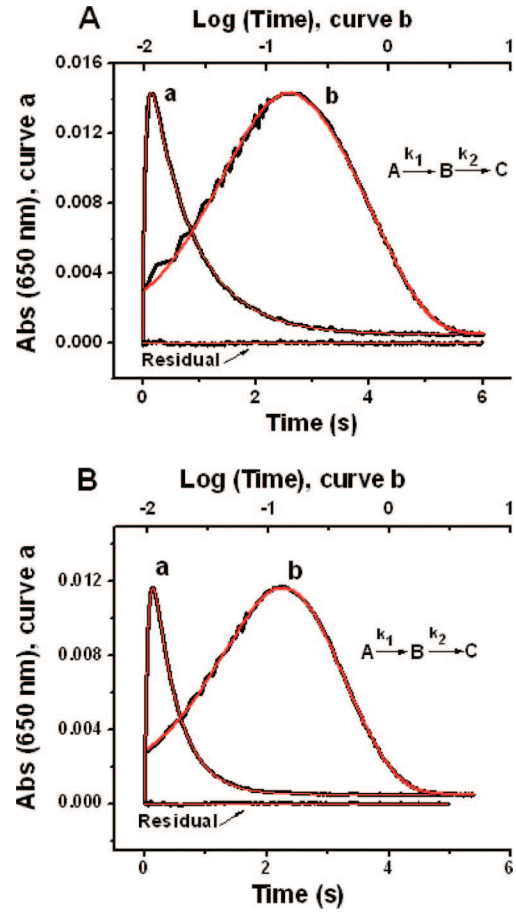

Figure 9. Stopped-flow absorbance versus time (curve a) and log(time) (curve b) for O_2 oxidation of Fe^{2+} prebound to variants no. 1 (panel A) and 2 (panel B) containing 48 Fe^{2+}/shell. Fitted curves are shown in red. The rate constants from curve-fitting are $k_1 = 18.4 \pm 0.4\ s^{-1}$ and $k_2 = 1.29 \pm 0.02\ s^{-1}$ for variant no. 1 (Figure 9A) and $k_1 = 17.5 \pm 0.6\ s^{-1}$ and $k_2 = 2.49 \pm 0.06\ s^{-1}$ for variant no. 2 (Figure 9B) from eq 6 with the equations for the concentrations of species given elsewhere.[31] The stated rate constants and associated errors are averages and standard deviations, respectively, from curve fits to three separate kinetic runs. The residual is the difference between the fitted and experimental linear time curves. The conditions are the same as in Figure 8.

intermediate is virtually unchanged by the substitution Y29Q, 18.4 versus 17.5 s^{-1}, indicating that Tyr29 is not important kinetically for directing O_2 to the ferroxidase center. However, substitution of Tyr29 with Gln29 ~12 Å from the ferroxidase center in variant no. 2 increases the rate constant k_2 for decay of the peroxo intermediate by ~2-fold compared to variant no. 1, 2.49 s^{-1} vs 1.29 s^{-1}. Long range effects of substitutions have been noted previously for ferritins.[49,50]

To determine whether O_2 binds at or near the ferroxidase center in the absence of Fe^{2+}, an anaerobic solution of either variant no. 1 or 2 (0.5 μM) was exposed to 100% O_2 atmosphere while monitoring the protein fluorescence. No quenching of fluorescence from the presence of O_2 was observed (data not

(49) Grady, J. K.; Shao, J.; Arosio, P.; Santambrogio, P.; Chasteen, N. D. *J. Inorg. Biochem.* **2000**, *80*, 107–113.
(50) Trikha, J.; Theil, E. C.; Allewell, N. M. *J. Mol. Biol.* **1995**, *248*, 949–967.
(51) Douglas, T.; Ripoll, D. R. *Protein Sci.* **1998**, *7*, 1083–1089.
(52) Takahashi, T.; Kuyucak, S. *Biophys. J.* **2003**, *84*, 2256–2263.
(53) Levi, S.; Santambrogio, P.; Corsi, B.; Cozzi, A.; Arosio, P. *Biochem. J.* **1996**, *317*, 467–473.

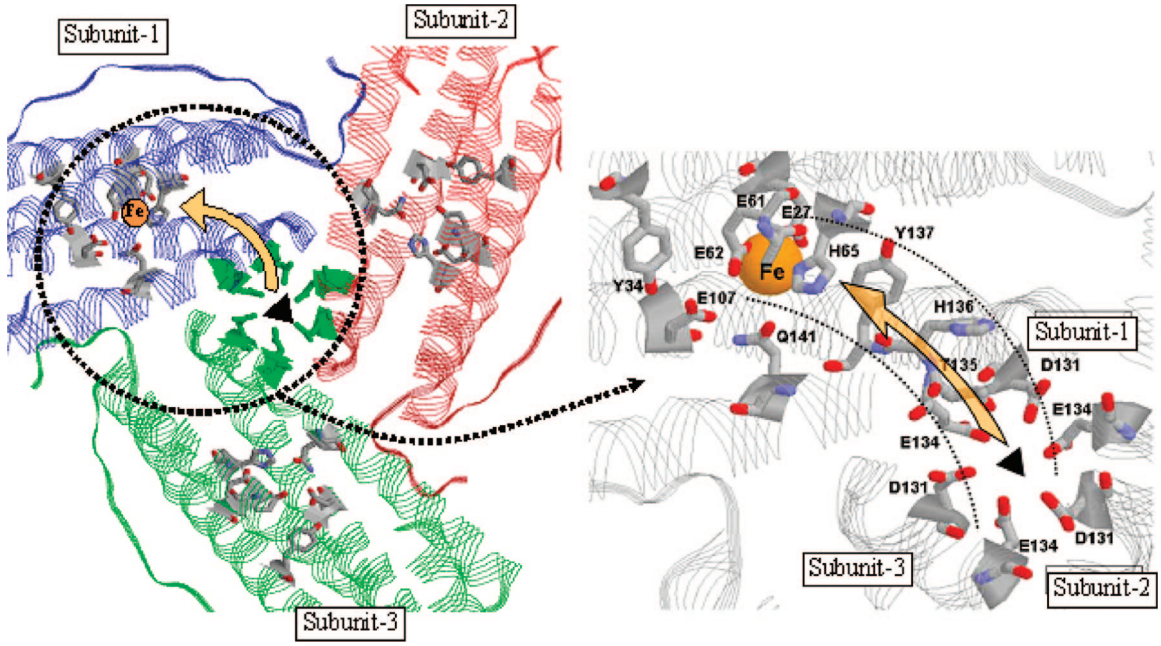

Figure 10. View from inside of the protein showing the suggested pathway for iron movement from the 3-fold channel to the ferroxidase center (left panel). Expanded view (right panel). The triads of 3-fold channel residues Asp131 and Glu134 are indicated. For clarity the three His118 and three Cys130 residues at the outer opening of the 3-fold channel are not shown. The ferroxidase center ligands His65, Glu27, Glu61, Glu107, and Glu62 and the residues Thr135, His136, and Tyr137 suggested to be involved in shuttling Fe^{2+} from the channels to the ferroxidase center are shown on the right. Residues Gln141 and Tyr34 involved in H-bonding in Figure 2 are also shown. The single Fe atom at the A-site (His-65 site) of the ferroxidase center is depicted in yellow.

shown), suggesting that O_2 by itself does not appreciably bind in the vicinity of Trp34 at the $P_{O2} \approx 1$ atm of the experiment.

Discussion

The migration of Fe^{2+} through the protein shell to the ferroxidase center is one early event occurring prior to formation of the μ-peroxodiferric intermediate in ferritin. The present data demonstrate that the 3-fold channels are the only pathways for rapid Fe^{2+} entry into the protein because no fluorescence quenching is observed with variant no. 3 lacking coordinating residues in the channels and because there is minimal quenching when Zn^{2+} is bound in the channels of variant no. 1 (Figure 5). Electrostatic calculations are consistent with Fe^{2+} migration to the ferroxidase center via a route involving these channels.[51,52] The initial contact and equilibrium binding of Fe^{2+} in the channels modeled by eqs 2 and 3 likely involves the residues His118 and Cys130 at the outer opening of the channels as previous work suggests[10,49,53,54] followed by the sequential migration to the deeper triads of Glu134 and Asp 131 residues. VO^{2+} binds at His118 and can be displaced by Fe^{2+},[49,54] and substitution of the His118 and Cys130 with alanine reduces iron uptake by the protein.[53] Recent X-ray structural data on Zn^{2+} (an Fe^{2+} surrogate) binding in the 3-fold channels of HuHF show metal occupancy of all of the three channel sites (His118 + Cys130, Glu134 and Asp131 sites)[10] in accord with the sequence of iron migration proposed here. It is not known which of these sites corresponds to the K_C measured in this work, but the soft character of the ligands of the His118 + Cys130 site would seem to be particularly well suited for binding Fe^{2+}. Figure 10 illustrates the putative pathway into the protein via the 3-fold channel and across the interior of the protein to the ferroxidase center. The residues Thr135, His136 and Tyr137 may be involved in guiding iron from the inner opening of the channel to the ferroxidase centers within the four-helix bundle. This path on the protein interior is a somewhat more direct route than that previously postulated.[17,51]

Fe^{2+} entry into the protein likely involves ligand exchange reactions between coordinated water of $Fe(H_2O)_6^{2+}$ and the Asp131 and Glu134 residues of the channels because the 6.2 Å diameter of the aqua Fe^{2+} ion exceeds the 3−4 Å diameter of narrowest section of the channels. Such exchange reactions would enable the Fe^{2+} to overcome the restrictive porosity of the channels as proposed by Raymond and co-workers.[21,25] A gated process allowing the preferential passage of iron could also be operable as suggested by experiments employing mutagenesis and chaotropic agents.[26−28] "Breathing" of the channels probably accounts for the ability of slightly larger (7−9 Å diameter) nitroxide spin probes to diffuse into ferritin, albeit at rates 10^6-fold slower than that of Fe^{2+} observed here, a process that is also inhibited by Zn^{2+}.[55]

The stopped-flow fluorescence quenching data of Figures 6 and 7 reveal that binding of Fe^{2+} to the ferroxidase center occurs rapidly with a hyperbolic dependence of the rate characteristic of facilitated diffusion,[45,46] in accord with a model in which Fe^{2+} is complexed by the channels and passed through them. Because ligand exchange/substitution reactions of Fe^{2+} chelates typically occur on the microsecond time scale[56] compared to the millisecond kinetics observed here, diffusion is most likely the rate limiting step for iron to bind at the ferroxidase center; thus, we equate the measured value of the rate constant $k_d = 216\ s^{-1}$ from Figure 7 and eq 2 with the rate constant for diffusion (or its lower limit). When the channels are saturated with Fe^{2+}, the maximal rate of diffusion across the protein shell

(54) Hanna, P. M.; Chasteen, N. D.; Rottman, G. A.; Aisen, P. *Biochemistry* **1991**, *30*, 9210–9216.
(55) Yang, X.; Arosio, P.; Chasteen, N. D. *Biophys. J.* **2000**, *78*, 2049–2069.
(56) Wilkins, R. G. *Kinetics and Mechanism of Reactions of Transition Metal Complexes*; VCH: Weinheim, 1991; p 202.

occurs with a half-life of 3 ms (or less), consistent with a previous multimixing stopped-flow study predicting that it be less than ~50 ms for the wild-type protein[29] and in accord with it being less than the half-life of ~50 ms for the formation of the peroxo complex in variant no. 1 under aerobic conditions for both protein and iron solutions (Figure S6).

A more detailed model for iron migration down the channels of ferritin is not easily formulated because it involves a combination of Fickian diffusion, drift forces from the electric field gradient on the protein surface,[51] fluxional character of the channels[26−28] and the dynamics of ligand exchange reactions within the channels.[21,25] If we assume that Fickian diffusion solely applies, an estimate of the "apparent diffusion coefficient" can be obtained. We equate the first-order half-life from the kinetics measurements to the time for half of the Fe^{2+} to travel the thickness of the protein shell d through a one-dimensional random walk process,[45] namely $t_{1/2} = (\ln 2)/k_d = d^2/(2D(0.67)^2)$ or $D \approx (k_d d^2)/(2 \ln 2(0.67)^2) = (k_d d^2)/0.62$. By substituting $k_d = 216\ s^{-1}$ and $d = 12$ Å (corresponding to the length of the narrowest region of the channel), into the above equation, we obtain $D \approx 5 \times 10^{-16}\ m^2/s$.[57] This value of D is considerably smaller than the measured diffusion coefficient for $Fe(H_2O)_6^{2+}$ in water ($D = 7.0 \times 10^{-10}\ m^2/s$).[58,59] If we correct the diffusion coefficient in water for the small fraction (0.0005) of the external surface area of the protein shell occupied by the openings of the eight funnel shaped channels, each having a cross-sectional area of ~25 Å^2,[51] we obtain a predicted value of $D \approx 3.5 \times 10^{-13}\ m^2/s$. This latter value corresponds to that expected for the unimpeded movement of the Fe^{2+} through the channels by a completely random walk process where the total cross-sectional area of the channels (assumed to be rigid pipes) and the viscosity of water are the only factors limiting the rate of transport into the protein shell. The estimated apparent diffusion coefficient of $5 \times 10^{-16}\ m^2/s$ from the value of k_d is nearly 1000-fold slower than the predicted value of $D \approx 3.5 \times 10^{-13}\ m^2/s$, further emphasizing the importance of other factors in affecting the movement of iron down the channels.

The ~10-fold greater conditional constant for Fe^{2+} binding at the ferroxidase centers compared to the channel binding sites ($K_F \approx 10^6\ M^{-1}$ vs $K_C \approx 10^5\ M^{-1}$) is consistent with the ferroxidase center being a thermodynamic sink for Fe^{2+}, favoring the translocation of iron to the center where oxidation takes place. The binding of Fe^{2+} in both instances is entropically driven (Figure 4 caption). That only ~12 of the 24 ferroxidase centers bind Fe^{2+}in variant no. 1 (Figures 3, 4 and S5) compared to all 24 Fe^{2+} centers for the WT protein[24] was unexpected in that the two proteins appear to fold similarly (Figures S1 and S2). However, a similar phenomenon has been observed with mitochondrial ferritin (MtF) which has the same ferroxidase center residues and overall structure as human H-chain ferritin.[60] Only 12 of the 24 ferroxidase centers of MtF bind iron and are catalytically active.[61] The origin of this effect in WT MtF and the variant no. 1 of HuHF is unclear.

The rate constant $k_d = 216\ s^{-1}$ reported here for diffusion of Fe^{2+} through the 3-fold channels to the ferroxidase center of human H-chain is at variance with the 540-fold smaller value of $0.40\ s^{-1}$ reported for the transfer of Fe^{2+} down the channels of horse spleen ferritin to the protein cavity where it reacts with encapsulated ferricyanide, $K_3Fe(CN)_6$, to form Prussian Blue, $KFe[Fe(CN)_6]$.[34] The rate constant of $0.40\ s^{-1}$ ($t_{1/2} = 1.7$ s) cannot correspond to migration of iron across the protein shell because it is *smaller than* the recently measured rate constant of $17.7\ s^{-1}$ ($t_{1/2} = 39$ ms) for formation of the peroxodiferric complex in horse spleen ferritin.[33] In the Prussian blue study, the authors suggest that Fe^{2+} might rapidly bind to the ferroxidase site and then slowly transfer to the "core" $K_3Fe(CN)_6$, thus accounting for the low rate of formation of $KFe[Fe(CN)_6]$.[34] In any case, the kinetics observed in the Prussian blue experiment are considerably more complex than those reported here and do not appear to be a true measure of diffusion of Fe^{2+} across the ferritin shell.

Our data do not support the hypothesis[37] that the "1-fold" channels are important pathways for O_2 penetration to the ferroxidase center (Figures 8 and 9). Tyr29 at the entrance to these channels (Figure 1D) does not have a functional role because essentially identical rates of formation of the peroxo intermediate for the control variant no. 1 and the Y29Q variant no. 2 are obtained ($k_1 = 18.4 \pm 0.4$ vs $17.5 \pm 0.6\ s^{-1}$, respectively) when O_2 is rapidly mixed with the protein prebound with Fe^{2+} (Figures 8 and 9). Thus, O_2 must penetrate to the ferroxidase centers faster than the millisecond time scale of our experiments and therefore does not influence the rate of Fe^{2+} oxidation. Oxygen has been shown to travel through protein matrices at near diffusion controlled rates.[62]

Finally, we note that the substitution Y34W influences both the thermodynamic and kinetic properties of the human H-chain ferritin even though the CD and melting properties of the protein are changed little by the substitution (Figures S1 and S2). Not only is the stoichiometry of Fe^{2+} binding reduced from 24 to 12 Fe^{2+}/shell (Figures 3, 4 and S5), the rate constant for formation of the peroxo diFe^{3+} complex under aerobic conditions is reduced as well, from $48.1\ s^{-1}$ per 24 ferroxidase sites for the WT protein to $13.8\ s^{-1}$ per 12 ferroxidase sites for variant no. 1 (Figure S6), corresponding to a reduction by a factor of 1.7 in rate constant per ferroxidase site. A similar reduction in the rate of iron uptake has also been reported for variant Y34F of HuHF.[14] Elimination of the H-bond from Tyr34 to the ligand Glu-107 (Figure 2) by the substitution Y34W or Y34F may be partly responsible for the observed changes in the properties of the protein. Despite these differences, the main conclusions derived from the present study likely apply to the wild type protein, namely that Fe^{2+} diffusion is rapid and occurs through the eight 3-fold channels and that Tyr29 is not important for O_2 diffusion into the protein.

In summary, our experiments with Y34W variants of human H-chain ferritin have provided new insights into the very early events of iron deposition in ferritin. In particular, the rate at which Fe^{2+} arrives at the ferroxidase center has been measured directly for the first time and shown to be ~15-fold faster than

(57) The equation used here differs by a factor of ~16 from the relationship $D \approx (k_d d^2)/\pi^2$ previously used to estimate D in other studies of the diffusion of Fe^{2+} and nitroxides into ferritin.[34,55] This relationship is not appropriate since its derivation is based on the relaxation time τ_{ss} for reaching a steady state in diffusant concentration with distance rather than the half-life, $\tau_{1/2}$, for material transport.[45] Therefore, in previous work[34,55] the "apparent Fickian diffusion coefficients" were underestimated by a factor of ~16.

(58) Leaist, D. G.; Hao, L. *J. Chem. Soc., Faraday Trans.* **1994**, *90*, 133–136.

(59) Spiro, M.; Creeth, A. M. *J. Chem. Soc., Faraday Trans.* **1990**, *86*, 3573–3576.

(60) Langlois d'Estaintot, B.; Santambrogio, P.; Granier, T.; Gallois, B.; Chevalier, J. M.; Precigoux, G.; Levi, S.; Arosio, P. *J. Mol. Biol.* **2004**, *340*, 277–293.

(61) Bou-Abdallah, F.; Santambrogio, P.; Levi, S.; Arosio, P.; Chasteen, N. D. *J. Mol. Biol.* **2005**, *347*, 543–554.

(62) Coppy, M.; Jameson, D. M.; Alpert, B. *FEBS Lett.* **1981**, *126*, 191–194.

the rate of aerobic Fe^{2+} oxidation in the variants studied, $t_{1/2}$ = 3 vs 50 ms (Figure S6). Moreover, the 3-fold channels have been demonstrated kinetically to be the only pathways for rapid iron entry into the protein by a process involving facilitated diffusion. O_2 diffusion into the protein does not depend on Tyr29 and occurs on a time scale much faster than milliseconds.

Acknowledgment. This work was supported by Grant No. R01 GM20194-33 from the National Institute of General Medical Sciences (N.D.C.) and by Grant No. MIUR-PRIN 2006 (P.A.). The authors thank Prof. Martin Case of the University of Vermont for measuring the CD spectra and melting curves for the WT and variant no. 1 proteins.

Supporting Information Available: Circular dichroism spectra of apo-HuHF and apo-variant no. 1, kinetic data for test reactions of the stopped-flow instrumentation, anaerobic ultraviolet spectrometric titration of apo-variant no. 1 with Fe^{2+}, stopped-flow absorbance-time curves for aerobic addition of Fe^{2+} to apo-variant no. 1 and to apo-HuHF, derivation of the Fe^{2+} binding isotherm (eq 1) and deriviation of the kinetic model for diffusion (eq 3). This information is available free of charge via the Internet at http://pubs.acs.org/.

JA8054035